Date of publication xxxx 00, 0000, date of current version xxxx 00, 0000.

Digital Object Identifier 10.1109/ACCESS.2017.DOI

Inferring Cortical Connectivity from ECoG Signals Using Graph Signal Processing

SIDDHI TAVILDAR[1,2], BRIAN MOGEN[2,3], STAVROS ZANOS[2,4,5], STEPHANIE SEEMAN[2,6], STEVE PERLMUTTER[2,4,6], EBERHARD FETZ[2,4,6] AND ASHKAN ASHRAFI[1,2,7], (Senior Member, IEEE).

[1]Computational Science Research Center, San Diego State University, San Diego CA, USA.
[2]Center for Neurotechnology, Seattle WA, USA.
[3]Department of Bioengineering, Univ of Washington, Seattle WA, USA.
[4]WA National Primate Research Center, Univ of Washington, Seattle WA, USA.
[5]Center for Bioelectronic Medicine, Feinstein Institute for Medical Research, Manhasset NY, USA.
[6]Dept. Physiology & Biophysics, University of Washington, Seattle WA, USA.
[7]Department of Electrical and Computer Engineering, San Diego State University, San Diego CA, USA.

Corresponding author: Siddhi Tavildar (e-mail: stavildar@sdsu.edu).

This paper has been supported by the NSF Center for Neurotechnology (NSF Grant Number: EEC-1028725)

ABSTRACT A novel method to characterize connectivity between sites in the cerebral cortex of primates is proposed in this paper. Connectivity graphs for two macaque monkeys are inferred from Electrocorticographic (ECoG) activity recorded while the animals were alert. The locations of ECoG electrodes are considered as nodes of the graph, the coefficients of the auto-regressive (AR) representation of the signals measured at each node are considered as the signal on the graph and the connectivity strengths between the nodes are considered as the edges of the graph. Maximization of the graph smoothness defined from the Laplacian quadratic form is used to infer the connectivity map (adjacency matrix of the graph). The cortical evoked potential (CEP) map was obtained by stimulating different electrodes and recording the evoked potentials at the other electrodes. The maps obtained by the graph inference and the traditional method of spectral coherence are compared with the CEP map. The results show that the proposed method provides a description of cortical connectivity that is more similar to the stimulation-based measures than spectral coherence. The results are also tested by the surrogate map analysis in which the CEP map is randomly permuted and the distribution of the errors is obtained. It is shown that error between the two maps is comfortably outside the surrogate map error distribution. This indicates that the similarity between the map calculated by the graph inference and the CEP map is statistically significant.

INDEX TERMS Brain connectivity, Cortical Connectivity, Electrocorticography (ECoG), Graph Learning, Graph Signal Processing, Neural Signal Processing

I. INTRODUCTION

THE studies conducted over the past few decades prove the existence of a large number of highly connected cortical networks, allowing communication between spatially separated brain regions. Technological developments have served as catalyst for the growing interest in the detection and understanding of connectivity in the brain. Brain activity is being investigated using hemodynamic techniques such as functional Magnetic Resonant Imaging (fMRI) [1], [2], [3] and electrophysiological techniques such as electroencephalography (EEG) [4], [5] and Electrocorticography (ECoG) [6], [7]. Analysis of brain connectivity networks has a potential to advance our understanding of the human brain and to offer improvements in the management of various neurological disorders.

Graphs are mathematical representation of networks. In the last decade, representation of brain as a graph where different brain regions are considered as vertices and edges indicate functional dependence between their activities, has been introduced and used rigorously [8]. Time varying partial directed coherence on high resolution EEG signals have been used to demonstrate the significance of brain network

analysis in revealing the important information regarding the dynamics of cortical networks [4]. Additional study [9] proposes a method for computing structural complexity of the graphs based on their signal transformations. In this method, the connectivity graphs are constructed using time-varying phase locking value in EEG signals. However, EEG has limited spatial resolution because of volume conduction effect [10]. In the analysis of functional connectivity of brain many researchers have also preferred fMRI [11], [12], [13], [14], [15], [16]. Although fMRI provides high spatial resolution, it is limited in temporal resolution. Moreover, fMRI may be inadequate to interpret the underlying neuronal activities [10].

ECoG is the recording of electrical activity directly from the cortical surface of a subject. It is an invasive method that provides high quality cortical signals with better spatio-temporal resolution than EEG [10]. Many researchers have used ECoG signals to investigate the brain connectivity. Correlations between the ECoG signals recorded at different electrodes are considered as a measure of functional connectivity to locate the epileptic zone [17]. ECoG signals of the finger flexion experiment are used to assess the brain connectivity in resting and task state by generating the functional connectivity graph based on phase synchronization theory [18]. In more recent work Ko *et al*. have used high gamma band power fluctuations in human ECoG signals to describe cortical connectivity [19] . Another study estimates the cortical connectivity based on dipole source analysis of evoked ECoG data in swines [20]. In a study involving Alzheimer's disease ECoG recordings and local field potentials recorded from sensory cortex in rats are used [21]. Additional studies have shown that fMRI and high gamma ECoG are reliable tools to support pre-surgical mapping of cortical functions [22].

There are several ways of determining the connectivity of sites in the brain using electrical signals at various locations relative to the source activity measured from electrodes at the neural population scale. Gross measures or related activities like cross-channel correlation [23], [24], [25] pick out time-amplitude similarity between channels and coherence [26], [27], [28] is commonly used to analyze frequency-dependent connections in spontaneous data [8]. Unfortunately coherence and correlation measures do not consistently provide the same robust description of connectivity gained from stimulation methods. Multivariate Vector Autoregressive (MVAR) model have been used in many different brain functional connectivity analyses. The core concept of the MVAR is finding the causality between recorded brain signals. Granger causality analysis [29], [30], which is based on the MVAR provides a framework for directional connectivity analysis. The definition of causality motivates numerous methodologies proposed for estimating the directed connections. These include directed transfer function [31], directed information [32], transfer entropy [33], vector auto-regressive analysis [34], [35], structural equation modeling [36], structural vector auto-regression [37]. However, those maybe difficult to interpret with confidence [38], [39].

Electrical stimulation can be applied to directly activate underlying neural tissue and evoke spatio-temporal patterns of activation at connected sites [39], [40]. Short latency [3-30ms] responses to this electrical stimulation encompass mono and poly-synaptic connections between sites whose amplitudes scale with the strength of connection [41]. The Cortical Stimulation-Evoked Potential (CEP) map is a commonly used description of cortical connectivity when anatomical measures are not available.

Graph signal processing (GSP), in which the concepts and algorithms of traditional digital signal processing are implemented on a graph signal (values on the vertices of the graph) is an emerging field of signal processing [42], [43]. Although the graph representation is useful in numerous fields, it is often not readily available. Construction of meaningful graphs from the data observations plays an important role in the representation and use of GSP. The process of building a meaningful graph from data observations is crucial and has been given many names as graph learning, network topology inference or graph inference. Different approaches have been developed for graph inference from signal observations. One approach is graph inference methods that employ smoothness property (where the neighboring nodes tend to have similar values) of the graph signals. The methods presented in [44] and [45] estimate graph Laplacian matrix that maximizes the smoothness of the graph signal. The more recent work based on the smoothness of the graph signal is by Chepuri *et al*. to infer the sparse graph structure using edge selection strategy [46]. In the work by Egilmez *et al*., a method to estimate graph Laplacian matrix from data under structural connectivity constraints is explained [47]. Other studies like [48], [49], [50] have used diffusion based methods for graph inference. In these methods the graph topology is inferred from the signals assumed to be diffused on the graph. In a recent study, the graph and signal on graph are jointly modeled using compound Markov Random Field. The underlying graph is inferred using Maximum A posteriori (MAP) estimator [51]. The detailed review of different graph inference methods is covered in [52] and [53].

In this paper we use graph inference algorithm by [44] on spontaneous ECoG signals of primates to extract the graph structure that describes the topological properties of the underlying brain network. The past research reveals that the anatomical and functional cortical connectivity graphs inferred using electrophysiological data of primate and human brain exhibit small world network properties [54], [55], [56]. The graph inference algorithm based on smoothness prior is more suitable for graphs whose edges represent some global relationships such as small world and Barabási-Albert graphs compared to graphs whose edges are less structured and have weaker global relationship such as Erdős Rényi graph [44]. Moreover, the notion of similarity between the signal entities considered in the smooth signal prior is congruous with the earlier methods used for brain connectivity analysis. This algorithm uses the multi-variate similarity between signals to

infer the connectivity whereas spectral coherence and Pearson correlation employ bi-variate similarity methods [57].

The proposed mathematical framework provides a description of cortical connectivity that is more similar to the stimulation-based measures than spectral coherence. Therefore, we expect to have connectivity maps closer to the CEP map than the ones spectral coherence infers. We compared the connectivity maps created from three canonical coherence bands and graph inference to the CEP map. In the animals under study (monkey U and monkey Q), we found that the inferred graph is a close representation of the CEP map.

It is important to note that this approach does not analyze the temporal variation of the map. Temporal information can identify the directionality of the connections, from which the causal relationship between signals can be inferred. Nevertheless, methods that analyze undirected correlations, such as spectral coherence, are still widely applied to ECoG activity to deduce connectivity maps over time. The method presented in this paper can be categorized as one of these methods that infers undirected connectivity maps from sliding windows of ECoG activity recorded from multiple cortical sites. The new method is compared with maps derived from spectral coherence analyses.

The rest of the paper is organized as follows, section II, explains the experimental set-up and data acquisition methods. Section III describes the mathematical methods used to infer the connectivity maps in detail. Section IV explains graph inference method for analyzing cortical connectivity. Section V considers the application of the mathematical methods on the data obtained from monkey U and monkey Q (animals under study) and compares the performance of the mathematical methods with the CEP map. Section VI contains the analysis of the obtained results, followed by the conclusions of the paper in section VII.

II. EXPERIMENT SET UP AND DATA ACQUISITION

In this section the experiment set up and the process of data acquisition from the subject is explained. Both ECoG signals and Cortical Evoked Potentials (CEPs) were recorded from the same animal under study. The ECoG signals were used to infer the cortical connectivity and the CEPs were used to validate the proposed graph inference method.

A. EXPERIMENT SET UP AND ECOG DATA ACQUISITION

The animals under study were implanted with a grid of custom-made Platinum-Iridium Rod dual-plug electrodes consisting of 15 electrode sites per hemisphere for monkey U and 13 electrode sites per hemisphere for monkey Q prior to experimentation. The 3×5 grid with 3mm center-to-center spacing was arranged over the primary motor and sensory cortex using stereotaxic coordinates [58]. The surgery was done under sterile conditions and all protocols were approved by the University of Washington Animal Care and Use Committee. The activity was recorded between one electrode per

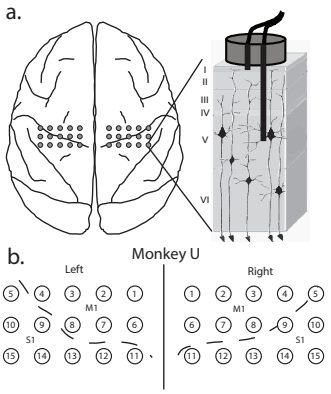

FIGURE 1: Monkey U electrode implant schematic (adapted from [58]) (a) Top-down view of brain showing the approximate position of each dual electrode. The depth electrode punctured the dura and the surface electrode was placed above the dura. (b) Numbered electrode sites for Monkey U

site and a distant reference electrode (Fig. 1, adapted from [58]). ECoG signals were recorded from an awake Monkey U while it was performing a standard center-out task using manipulandum in a shielded primate recording booth using a Grapevine Neural Interface System from Ripple [Salt Lake City, UT] at 30 KHz (down-sampled to 5 KHz post-hoc). In case of monkey Q, the ECoG signals were recorded using amplifiers from Guger Technologies [Graz,Austria] at 4.8 KHz while the animal was sitting quietly in the shielded primate recording booth. The experiment consisted of 35 recording sessions (trials) for monkey U and 19 recording sessions (trials) for monkey Q. In each session spontaneous neural activities were recorded for $10 - 30$ minutes before stimulation protocols were applied. All data analysis was performed using custom MATLAB software.

B. CORTICAL EVOKED POTENTIALS

Electrical stimulation was applied following a stimulation ramp procedure outlined in [58]. Briefly, a set of eight anodal-first biphasic constant current stimulation pulses was applied between the depth and surface electrodes at a site causing a focal electrical activation of neural tissue. The stimulation was ramped from 0 to $700\mu A$ in $100\mu A$ increments every 300ms to allow neural circuits time to return to baseline between stimulations. Fifty stimulation ramps were applied to every electrode in the hemisphere over the course of two sessions. Stimulation events were aligned in time and grouped by channel and intensity for further analysis.

Ramped stimulation at a site produced a graded stimulus response across the grid of electrodes which was used to characterize the response from different channel pairs. This direct electrical stimulation produces short latency activations, Cortical Evoked Potentials (CEPs) at cortical locations that are directly connected via synaptic pathways indicating a direct functional connectivity that can be influenced by a variety of plasticity protocols [58].

To obtain standardized CEP measures across the network

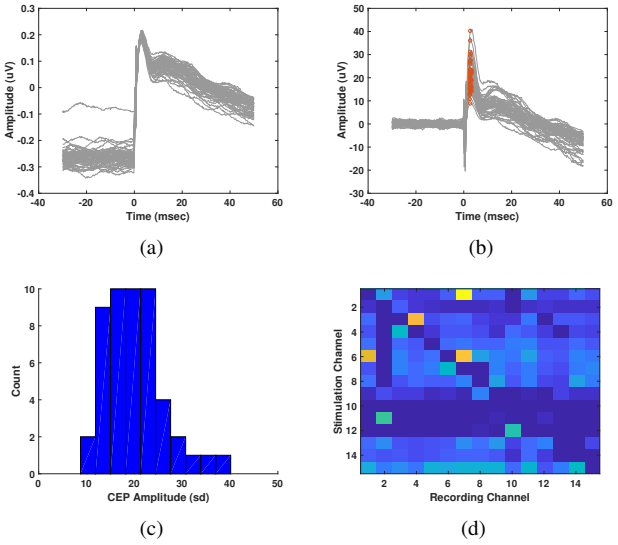

FIGURE 2: Cortical Evoked Potential (a) Raw traces, Stim Channel :R04, Response Channel: R01 (b) Z Scored Traces, Stim Channel :R04, Response Channel: R01 (c) CEP amplitudes, Stim Channel :R04, Response Channel: R01 (d) CEP connectivity map.

we first normalized the amplitude of the responses on all channels by baseline correcting and Z-scoring each stimulation response using the 20ms of data preceding each stimulation. The first positive and negative peak and respective post-stimulus latency were extracted from the individual trials using MATLAB's built-in peak-finding algorithm. The responses were then averaged across trials to obtain a single amplitude value per site. We discarded peaks that did not exceed three standard deviations Fig. 2(c). The amplitude of these normalized responses is a direct measure of the strength of the synaptic connectivity between the two sites. The data from the right hemisphere of monkey Q was unavailable for this study.

III. MATHEMATICAL METHODS FOR INFERRING CONNECTIVITY

Spectral coherence which is computed using the power spectral density of the signals is one of the common methods for inferring connectivity using the ECoG data. The mathematics and shortcomings of the spectral coherence method in comparison with the theory of graph inference method are analyzed in this section.

A. SPECTRAL COHERENCE ANALYSIS

Spectral coherence is the most popular mathematical method for inferring functional and anatomical connections between neural signals using spontaneous recordings. It estimates how well two signals correspond at different frequencies as given by the following formula.

$$C_{xy}(f) = \frac{|P_{xy}(f)|^2}{P_{xx}(f)P_{yy}(f)} \tag{1}$$

where, f is frequency in Hz, $P_{xy}(f)$ is the cross-spectral density between signals $x(t)$ and $y(t)$, $P_{xx}(f)$ is the spectral density of signal $x(t)$ and $P_{yy}(f)$ is the spectral density of signal $y(t)$.

For our analysis, the continuous frequency spectrum was binned into canonical frequency bands [59], alpha ($8-12$ Hz), beta ($12-30$ Hz) and gamma ($30-58$ Hz) with notches at line noise (60 Hz) and its harmonics. The mean value in each band was used to describe the connectivity present in spontaneous recordings.

The phase difference between two signals can express the relative displacement between the two signals. Phase is generally used to determine the temporal dependency of the signals on each other which can be very useful in finding the connectivity of the signals.

In the spectral coherence calculation, only the magnitude spectrum of the signals is considered while the phase spectrum is ignored. The nature of ECoG signals is such that the phase of the signal changes even in a small time duration. Fig. 3(a) shows the ECoG signal with it's 40 ms delayed version. Although the magnitude spectrum (Fig. 3(b)) of the time-shifted signal remains the same, there is a significant change in the phase of the delayed signal (Fig. 3(c)). The studies conducted in the past have used the phase synchronization information from the EEG signals to explore the neural activity in epileptic patients [60]. Additionally, phase lag index was introduced and used as a measure of functional connectivity [61]. However, the spectral coherence considers only the magnitude spectrum of the signals (from the formula in 1), therefore the phase information is eliminated. This reduces its effectiveness for inferring connectivity.

B. GRAPH INFERENCE

Consider an undirected weighted graph $\mathbf{G} = (V, \mathbf{A})$ where $V = \{v_1, v_2, ...v_n\}$ is the set of n vertices (or nodes) and $\mathbf{A} = (a_{ij})$ is the weighted adjacency matrix of size $n \times n$, where the entries of the matrix $a_{ij} \geq 0$ are the weights. The graph signal (or signal on graph) is the representation of a structured data, where the signal values are associated with the vertices of a graph and their pair-wise relationships are represented by the adjacency matrix $\mathbf{A}$. Each weight a_{ij} of an edge from vertex v_i to vertex v_j indicates the degree of relation between the i^{th} signal entity to j^{th} signal entity. A neighbourhood of a vertex v_i is defined as the set of nodes indices connected to the vertex v_i and is denoted as $\mathcal{N}_i = \{j | a_{ij} \neq 0\}$. The degree of any vertex i is defined as the sum of all weights of the edges connected to that node, i.e., $d_i = \sum_{j=1}^{n} a_{ij}$. The degree matrix $\mathbf{D}$ is a diagonal matrix with the degree vector $d = \{d_1, d_2, ...d_n\}$ on it's main diagonal. With the known adjacency matrix, the graph Laplacian matrix is defined as

$$\mathbf{L} = \mathbf{D} - \mathbf{A}. \tag{2}$$

The graph Laplacian matrix of an undirected graph $\mathbf{G}$ is symmetric and positive semi-definite (the eigenvalues are

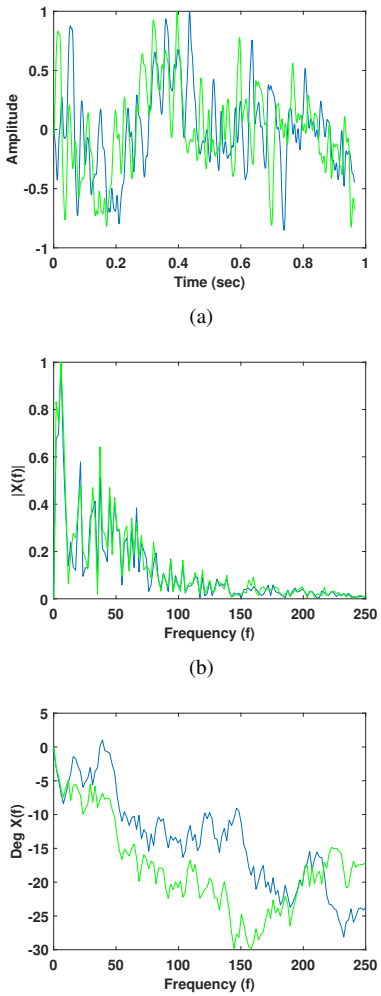

FIGURE 3: ECoG signal (blue) of length 1 sec and the same signal delayed by 40 ms (green) (a) Time Domain signals, (b) Magnitude spectrum of the signals, (c) Phase spectrum of the signals

non-negative). With this introduction to the key terms in graph signal processing, we move to the graph inference algorithm.

In their recent work, Dong *et al*. have proposed an algorithm for inferring the graph topologies from signal observations that depicts the intrinsic relationships between the data entities [44]. Specifically, the graph topology is inferred such that the observed signals have smooth variations on the graph.

The signal is considered smooth on a graph when the connected vertices have comparable signal values. The graph Laplacian quadratic form or $\mathbf{x}^T\mathbf{L}\mathbf{x}$ is used to measure the smoothness of signal $\mathbf{x}$ on graph, i.e.,

$$\mathbf{x}^T\mathbf{L}\mathbf{x} = \sum_{i,j \in V} a_{ij}(x(i) - x(j))^2 \tag{3}$$

where $\mathbf{x} \in \mathbb{R}^n$ is the graph signal and $x(i)$ is the signal value at vertex i. If the signal $\mathbf{x}$ on the graph is constant, the graph Laplacian quadratic form is zero. If the weight between two vertices is small, regardless of the signal values, the graph Laplacian quadratic form is small. To maximize the smoothness property of the observed signals on the inferred graph, the graph Laplacian quadratic form (3) should be minimized. The Laplacian matrix is found by solving the following optimization problem [44]:

$$\begin{aligned} \underset{\mathbf{L},\mathbf{Y}}{\text{minimize}} \quad & ||\mathbf{X} - \mathbf{Y}||_2 + \alpha \operatorname{tr}(\mathbf{Y}^T\mathbf{L}\mathbf{Y}) + \beta||\mathbf{L}||_F^2 \\ \text{subject to :} \quad & \operatorname{tr}(\mathbf{L}) = n \\ & \mathbf{L}(i,j) = \mathbf{L}(j,i), \qquad i \neq j \\ & \mathbf{L}.\mathbf{1} = \mathbf{0} \end{aligned} \tag{4}$$

where, columns of $\mathbf{X} \in \mathbb{R}^{n \times p}$ contain the signal observations, $\mathbf{Y}$ is the noiseless version of the observation $\mathbf{X}$, n is the number of vertices on the graph, $\operatorname{tr}(.)$ is the trace of a matrix, $||.||_F$ is the Frobenius norm and α and β are positive numbers. The rightmost term in the objective of the optimization problem (4) is imposed as a penalty term to improve the numerical stability of the optimization problem and to control the sparsity of the solution. The parameter α controls the smoothness and the parameter β controls the sparsity of the inferred graph. The variable $\mathbf{Y}$ is introduced in the optimization to reduce the effect of the measurement noise in $\mathbf{X}$. The detailed description of the graph inference algorithm is given in [44]. Since the Laplacian matrix is symmetric, this algorithm is computationally limited to derive a symmetric connectivity matrix which is translated to an undirected graph.

IV. GRAPH INFERENCE FOR BRAIN CONNECTIVITY

To find the connections between different parts of the brain, we look for similar behavior/pattern in the ECoG signals. Techniques such as correlation, phase and frequency synchronization and mutual information have been used to determine the connectivity between different parts of the brain [17], [18], [19], [38]. We assume that the ECoG electrodes constitute the vertices of a graph and the inter-connections form the edges of the graph. The ECoG signals (or their processed versions as explained in the next section) are considered as the signal on the graph. The graph inference algorithm explained in Section III-B is employed to infer the underlying brain connectivity using ECoG signals. However, in the current setting, if the signal from one electrode is a slightly delayed version of the signal from another electrode, the graph inference algorithm explained in section III-B will consider these two electrodes as weakly connected or unconnected because the graph inference algorithm considers the point-to-point similarity of the signals. To mitigate this problem, we need a representation of the signal that considers both magnitude and phase spectrum. Therefore, instead of using the raw signals, we use the auto-regressive (AR) model coefficients.

A. PRE-PROCESSING OF ECOG DATA

The raw ECoG data is pre-processed before applying graph inference algorithm. To remove the artifacts generated by large movements, a threshold was applied that surpassed the 99.5^{th} percentile of the mean data. Pre-processing of the data includes low-pass filtering (with cut-off frequency 250 Hz), down-sampling to 2000 Hz and segmentation. The signals from ECoG electrodes are divided into one second epochs with 50% overlap. The segmentation is performed starting with the first sample of the signals without any particular cue. The overlapping is to avoid abrupt changes in the inferred graph connections.

B. AUTO-REGRESSIVE MODEL

The Auto-Regressive model is defined as:

$$y(n) = \sum_{i=1}^{p} a_i y(n-i) + e(n) \tag{5}$$

where, p is the model order; $y(n)$ is the signal to be modelled, a_i's are AR coefficients and $e(n)$ is Gaussian white noise. The system parameters, (a_i's) also known as AR coefficients, capture the magnitude as well as phase information. This will allow us to use the graph inference method in (4).

1) Order of the AR model

Selecting the optimum model order is crucial as too small model order may not be sufficient to represent the signal because of the poor resolution. Furthermore, too large model order may cause spurious peaks in the spectrum and can also increase the computational complexity. Several criteria that indicate the appropriate model order for a given data set have been proposed. We have used the Akaike's Information Criterion (AIC) which is an estimator of the relative quality of statistical models for a given set of data [62]. It is defined as:

$$\mathrm{AIC}(p) = N \log(\epsilon_p) + 2p \tag{6}$$

where, p is the model order; ϵ_p is the modelling error and N is the length of the data set.

For a randomly selected data segment, we computed the AIC values for model orders ranging from 2 to 30. The order after which there was a minimum change in the AIC values was selected as the candidate for optimum model order (Fig. 4(a)). This was repeated for 500 segments selected randomly from the entire data set. The distribution of the corresponding candidates for optimum model orders is plotted (Fig. 4(b)). The final optimum model order is selected that is separated by twice the standard deviation from the mean of the distribution. The AR modelling essentially converts an epoch of the ECoG signal of numerous samples into a short sequence (20 in this case) of numbers (the AR coefficients). The obtained 20 coefficients of the AR models are used for graph inference. In the proposed scheme, we are limited to undirected graphs due to the inherent limitation of the graph inference algorithm (4).

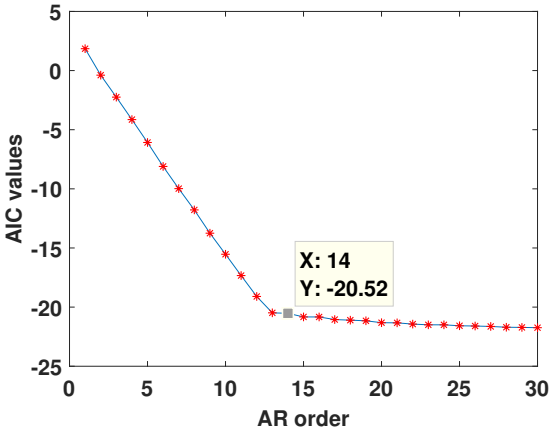

(a)

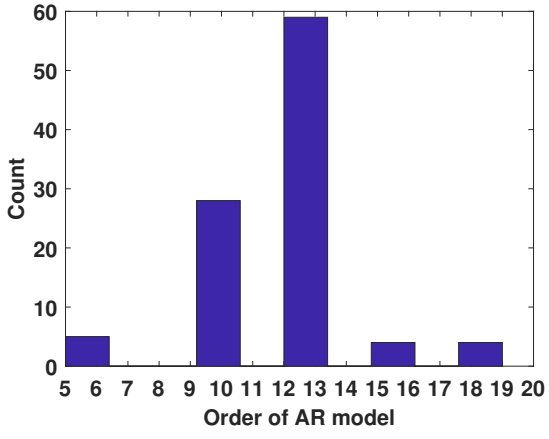

(b)

FIGURE 4: (a) Plot of AIC values of the AR models with increasing order. For current data segment, the candidate for optimum model order is 14. The changes in AIC values after 14 are negligible. (b) Distribution of the candidate model orders for 500 randomly selected segments of ECoG data.

C. CALCULATING THE ADJACENCY MATRIX

To find the underlying connections between the vertices of the graph, we need to find the adjacency matrix $\mathbf{A}$. The following major assumptions are considered for the graph inference algorithm:

1) The adjacency matrix $\mathbf{A}$ is symmetric.
2) There are no self-loops in the underlying graph, i.e, main diagonal of the adjacency matrix $\mathbf{A}$ is zero.
3) The similarity of the AR coefficients determines the weight of the connection.

The first assumption indicates that the graph is undirected. In a symmetric adjacency matrix, we have $a_{ij} = a_{ji}$. To this end, our focus is on finding the similarity in the activity of different cortical regions (functional connectivity).

The second assumption is based on the fact that the current algorithm would always consider that an electrode is connected to itself. This is because it will be using the similarity of the signal with itself to make a decision regarding

connectivity. Additionally, the strength of the self connection might also affect the strength of other connections negatively, making those negligible. Therefore, we assume the diagonal elements of the adjacency matrix to be zero, $a_{ii} = 0$.

By the third assumption, the underlying graph is formed to create the smoothest possible signal on graph. It is important to note here that the smoothness property is used to evaluate the connectivity. A smooth signal observation would result in more connected graphs while a less smooth signal observation would result in sparsely connected graphs. It should be noted that this statement is a sufficient condition not a necessary one. If a signal observation is smooth, the inferred graph is more connected. However, if a graph is more connected then we cannot conclude that the signal on the graphs is smooth.

The optimization problem in (4) is then solved for $\mathbf{Y}$ and $\mathbf{L}$ where $\mathbf{X}$ is the AR coefficients of the ECoG signals from all the recording electrodes. The values of parameters α and β are selected to give graphs that are 10% sparse to match the sparsity of CEP maps (10.98%) and coherence maps (9.3%). The objective is to infer the complete cortical connectivity map, which is not sparse. Therefore, as suggested in [44] the ratio of $\frac{\beta}{\alpha}$ that yields 10% sparsity in the adjacency matrix is selected by exhaustive search. After finding the graph Laplacian matrix $\mathbf{L}$, we can easily obtain $\mathbf{A}$ by using (2). The resultant graph is the measure of functional connectivity. The process is repeated for all segments and all recording sessions.

D. OCCURRENCE PROBABILITY

With the proposed algorithm, we have one inferred graph (adjacency matrix) per segment. A connection (neural pathway) between two parts of the brain may not appear in one segment as those sections may not have similar activity at that segment. However, if we see the occurrence of the connection in several segments, which means similar activity is observed at those sites more often, we can conclude that there could be a neural pathway between those two sites. This concept can be quantified by calculating the probability of occurrence of a nonzero weight between two sites of the brain. We call this occurrence probability (OC). To find the OC matrix, we first binarize the adjacency matrix $\mathbf{A}$ to obtain matrix $\mathbf{B}$. The binarization involves thresholding with a global threshold value for all the segments. The distribution of the weights calculated by the graph inference method follows a Poisson distribution. This is consistent with the brain connectivity maps computed using other analytical and physiological methods such as spectral coherence, correlation and CEPs [63] (refer Fig. 5). In fact, Fig. 5 shows that the distributions of the weights obtained from the graph inference method and the CEP map are closer to Poisson distribution than the distribution of the weights obtained from spectral coherence. This also shows the validity of the proposed method. The threshold was selected as the 5^{th} percentile of the distribution of weights of 10000 randomly selected segments; given the dense nature of the brain connectivity maps, we do not want to discard more connections. The weights less than the threshold were set to zero. With this strategy, there is a possibility that certain weaker connections are considered above the threshold value. However, these weaker connections get lower values in the calculation of occurrence probability as they occur infrequently. The average of the $\mathbf{B}$ matrices of all segments in a trial is defined as the occurrence probability matrix, $\mathbf{P}$

$$\mathbf{P} = \frac{\sum_{m=1}^{M} \mathbf{B}(m)}{M}, \tag{7}$$

where the entry p_{ij} of $\mathbf{P}$ is the probability of occurrence of a non-zero weight between sites i and j, $\mathbf{B}(m)$ is the binarized adjacency matrix of the m^{th} segment and M is the number of segments in the trial. High occurrence probability of a connection between two electrodes can be interpreted as the high probability of existence of a neural pathway. Therefore, we use the occurrence probability of the edges of the inferred graph as an indication of the existence of a functional connection between the electrodes.

The connectivity map is represented in the heat-map format. The occurrence probability maps from all trials are averaged to get a single connectivity map per hemisphere of the animal (see Fig. 7(b), 8(b) and 9(b)). The heat-map of the occurrence probability is a symmetric matrix where a non-zero number represents the probability of the presence of an edge in the entire trial. Higher values in the heat map correspond to more frequently occurring connections and lower values in the heat map correspond to less frequently occurring connection. A zero in the heat map means there is no connection found throughout all the segments in the whole data. Fig. 6 shows the important steps for computing the connectivity map using spontaneous ECoG data from the monkey. The two analytical measures of connectivity considered here are coherence map (bottom branch) and graph inference map (top branch). As shown in the block diagram, the pre-processing steps for both methods are the same. We repeated the same analysis for different frequency bands. This was achieved by dividing the band limited (≤ 250 Hz) signal further into canonical frequency bands: alpha ($8-12$ Hz), beta ($12-30$ Hz) and gamma ($30-58$ Hz) before performing the segmentation of the signals. The purpose of this analysis is to explore the effects of using entire spectrum for graph inference as opposed to using the information from different frequency bins like in spectral coherence method.

V. RESULTS

We have normalized connectivity maps for three measures of connectivity: CEP, coherence and graph inference. All maps are normalized to have values between 0 and 1. As explained in Section II-B, the CEP map is a directed graph with corresponding adjacency matrix $\mathbf{A}$ being non-symmetric. Nevertheless, both the analytical methods (coherence and graph inference) are computationally limited to find undirected adjacency matrix $\mathbf{A}$. Therefore, to have a fair comparison between all three, the directed (non-symmetric) CEP map

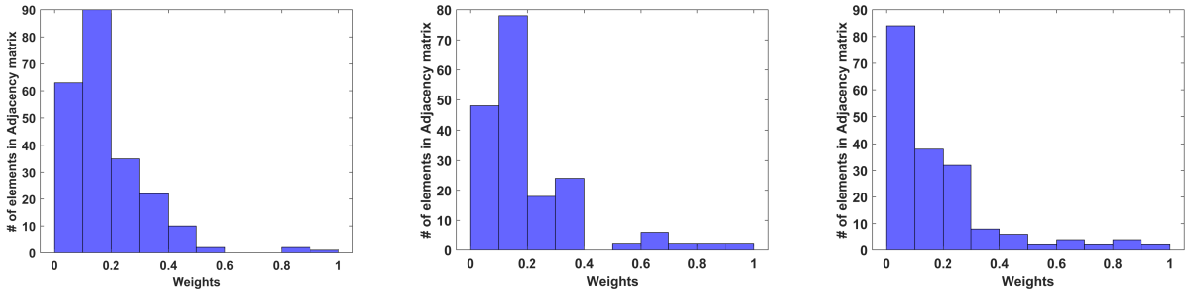

FIGURE 5: Distribution of weights in the adjacency matrix of brain connectivity maps using (a) cortical evoked potentials (CEP), (b) graph inference method and (c) spectral coherence method

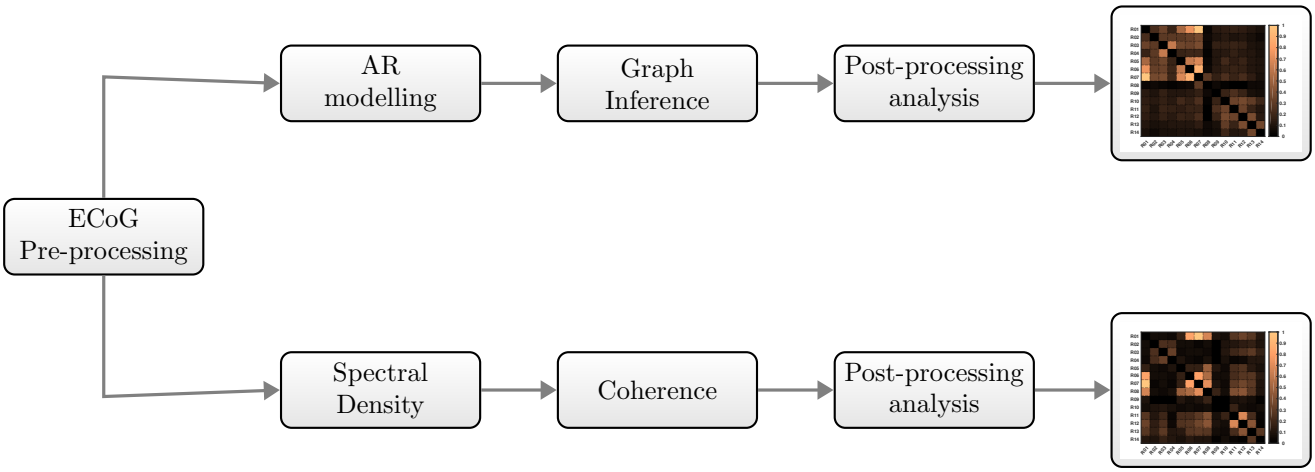

FIGURE 6: Block Diagram for computing the connectivity map from spontaneous ECoG data using analytical methods (graph inference in top branch and spectral coherence in bottom branch)

was converted to undirected (symmetric) CEP map by taking the average of the weights between electrode pairs.

The symmetric CEP maps for monkey U left hemisphere, monkey U right hemisphere and monkey Q left hemisphere are shown in Fig. 7(a), Fig. 8(a) and Fig. 9(a)). The results for normalized beta band coherence connectivity maps are in Fig. 7(c), Fig. 8(c) and Fig. 9(c) while the normalized graph inference connectivity maps are shown in Fig. 7(b), Fig. 8(b) and Fig. 9(b). Since the results from both alpha and gamma band coherence show connectivity patterns similar to beta band connectivity maps, they are not shown separately in the paper. The corresponding numerical results are documented in Table 1 and 2.

A. COMPARISON WITH CEPS

We compared the similarity of the connectivity maps created from three canonical coherence bands and graph inference to the symmetric CEP map using root mean square error (RMSE) to assess the performance of the methods. The true RMSE (TRMSE) between the CEP map and the obtained map is calculated using:

TABLE 1: Standardized parameter η for RMSE comparison.

Method	η (U-Left)	η (U-Right)	η (Q-Left)
Alpha Graph Inference	3.02	3.09	3.44
Beta Graph Inference	2.61	1.90	3.04
Gamma Graph Inference	2.32	2.28	2.51
Graph Inference (Total)	2.77	4.10	4.36
Alpha coherence	2.03	0.98	3.38
Beta coherence	1.52	0.96	2.19
Gamma coherence	2.06	1.68	0.65

$$\text{RMSE} = \sqrt{\frac{\sum_{i=1}^{n}\sum_{j=1}^{n}(c_{ij} - g_{ij})^2}{n^2}} \tag{8}$$

where, c_{ij} is the entry (i, j) of the normalized symmetric CEP map, g_{ij} is the the entry (i, j) of the map computed by one of the analytical methods (coherence or graph inference) and n is the number of electrodes.

We also compared the similarity of the connectivity maps created from three canonical coherence bands and graph inference to the symmetric CEP map using correlation coefficient. The correlation coefficient (r) between the CEP map

TABLE 2: Standardized parameter η for Correlation Coefficient comparison

Method	η (U-Left)	η (U-Right)	η (Q-Left)
Alpha Graph Inference	5.93	3.56	3.74
Beta Graph Inference	5.42	2.84	3.80
Gamma Graph Inference	4.94	2.76	4.04
Graph Inference (Total)	4.90	4.71	5.76
Alpha coherence	2.24	1.65	5.35
Beta coherence	2.27	2.47	2.93
Gamma coherence	2.23	2.39	2.31

TABLE 3: Performance evaluation Comparison

Monkey U- Left Hemisphere

Method	Precision	Recall	F-measure
Graph Inference	0.8462	1	0.9167
Coherence	0.8365	0.9886	0.9063

Monkey U- Right Hemisphere

Method	Precision	Recall	F-measure
Graph Inference	0.8750	1	0.9333
Coherence	0.8654	0.9890	0.9231

Monkey Q- Left Hemisphere

Method	Precision	Recall	F-measure
Graph Inference	0.9740	0.9868	0.9804
Coherence	0.9481	0.9865	0.9669

and the inferred map is defined as :

$$\rho = \frac{\sum_{i=1}^{n}\sum_{j=1}^{n}(c_{ij}-\overline{C})(g_{ij}-\overline{G})}{\sqrt{\left(\sum_{i=1}^{n}\sum_{j=1}^{n}(c_{ij}-\overline{C})\right)^2\left(\sum_{i=1}^{n}\sum_{j=1}^{n}(g_{ij}-\overline{G})\right)^2}} \tag{9}$$

where, c_{ij} is the entry (i,j) of the normalized symmetric CEP map C, g_{ij} is the the entry (i,j) of the map G computed by one of the analytical methods (coherence or graph inference). $\overline{C}$ is the mean of normalized symmetric CEP map C, $\overline{G}$ is the mean of the map G and n is the number of electrodes. Unlike RMSE, the similarity of maps is proportional to higher values of the correlation coefficient (ρ).

Additionally we evaluated the performance of graph inference and spectral coherence methods using $Precision$, $Recall$ and $F-measure$ metrics. These are calculated based on true positive (tp), false positive (fp) and false negative (fn) graph edges in the inferred analytical map(s) when compared with the CEP map as:

$$Precision = \frac{tp}{tp+fp} \tag{10}$$

$$Recall = \frac{tp}{tp+fn} \tag{11}$$

$$F-measure = \frac{2tp}{2tp+fn+fp} \tag{12}$$

The results are tabulated in Table 3. The values of the performance metrics were the same for all three canonical coherence bands. As seen in the Table 3, the values of $Precision$, $Recall$ and $F-measure$ for graph inference method slightly outperform the spectral coherence method.

B. STATISTICAL COMPARISON WITH SURROGATE GRAPHS

The TRMSE between the normalized symmetric CEP map and the map calculated by any method should be small if they represent similar functional connectivity. Nevertheless, a small TRMSE would not be enough to justify that the obtained connectivity maps represent the same underlying connectivity. We should show that the obtained TRMSE is statistically unique among all RMSEs between the calculated map and the random permutations of the CEP map (surrogate maps) [64] . In other words, if many surrogate maps are close to the calculated map so that their RMSEs are either close or smaller than the TRMSE, we cannot consider the calculated map as a genuine representation of the brain connectivity.

To evaluate the uniqueness of the calculated map, their RMSEs with 10,000 surrogate maps are calculated. We generated the surrogate maps by random permutation of the rows and columns of the CEP map. The distribution plots of these RMSE values for the left hemisphere of monkey U are shown in Fig. 7(d) and Fig. 7(e), with the vertical red line showing the TRMSE. The distribution plots of the RMSE values for the right hemisphere of monkey U are shown in Fig. 8(d) and Fig. 8(e), with the vertical red line showing the TRMSE. The distribution plots of the RMSE values for the left hemisphere of monkey Q are shown in Fig.9(d) and Fig. 9(e), with the vertical red line showing the TRMSE. The results in which the TRMSE value is well outside the distribution (smaller than the other RMSEs) is justified to provide a valid connectivity map that is closer to the CEP map.

The similar statistical comparison is performed with the correlation coefficient values. To evaluate the uniqueness of the calculated map, their correlation coefficients with 10,000 surrogate maps are calculated. We generated the surrogate maps by random permutation of the rows and columns of the CEP map. The distribution plots of these ρ values for the left hemisphere of monkey U are shown in Fig. 7(f) and Fig. 7(g), with the vertical red line showing the correlation coefficient of the original calculated map (true ρ). The distribution plots of the ρ values for the right hemisphere of monkey U are shown in Fig. 8(f) and Fig. 8(g), with the vertical red line showing the correlation coefficient of the original calculated map (true ρ). The distribution plots of the ρ values for the left hemisphere of monkey Q are shown in Fig. 9(f) and Fig. 9(g), with the vertical red line showing the correlation coefficient of the original calculated map (true ρ). The results in which the value of true ρ is well outside the distribution (higher than the other ρ's) is justified to provide a valid connectivity map that is closer to the CEP map.

We can use statistical standardization to quantify how the TRMSE (or true ρ) is positioned with respect to the surrogate distribution. The distance of the TRMSE (or true ρ) from the

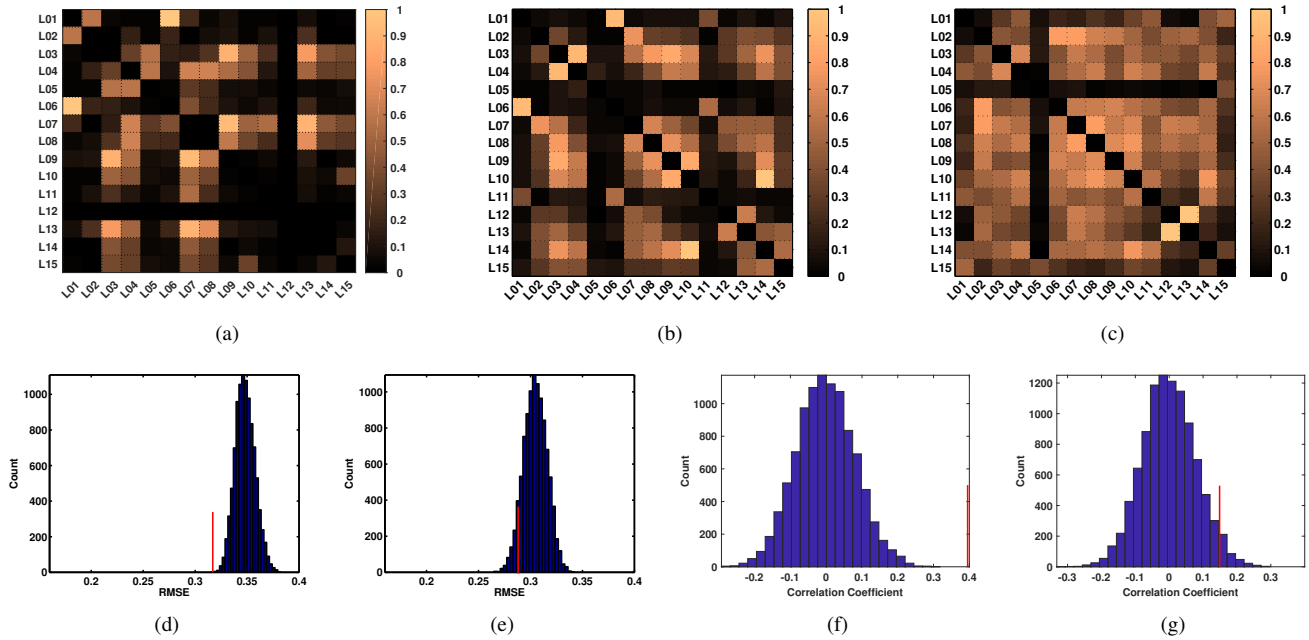

FIGURE 7: Monkey U, Left hemisphere connectivity results: (a) Cortical evoked potential (CEP) connectivity map (b) Cortical connectivity map using graph inference method (c) Cortical connectivity map using spectral coherence method (d) Surrogate maps (error) distribution for RMSE analysis using graph inference method; red line is indicating true RMSE (e) Surrogate maps (error) distribution for RMSE analysis using spectral coherence method; red line is indicating true RMSE (f) Surrogate maps (error) distribution for Correlation analysis using graph inference method; red line is indicating true correlation coefficient (g) Surrogate maps (error) distribution for Correlation Coefficient analysis using spectral coherence method; red line is indicating true correlation coefficient

mean of random distribution in terms of standard deviation is defined as the standardized parameter and is calculated as:

$$\eta = \frac{|r_m - r_t|}{\sigma} \tag{13}$$

where η is the standardized parameter, r_m is the mean of the surrogate distribution, r_t is the TRMSE (or true ρ) and σ is the standard deviation of the surrogate distribution.

The standardized parameters for RMSE comparison of the average connectivity maps across all 35 trials of monkey U and the average connectivity maps across all 19 trials of monkey Q are tabulated in Table 1 and the standardized parameters for correlation coefficient comparison of the average connectivity maps across all 35 trials of monkey U and the average connectivity maps across all 35 trials of monkey Q are tabulated Table 2. The higher the value of η, the closer the obtained map is to the CEP map. Although the η values for graph inference method in alpha, beta and gamma bands outperform the corresponding values of η in spectral coherence method, we prefer to use graph inference method on the entire band-limited ($\leq$ 250 Hz) data. This approach is computationally efficient and results in a frequency agnostic measure of connectivity. The connectivity results of the graph inference method in Table 3 and in Fig. 7, 8 and 9 are of the entire band-limited ECoG data.

VI. DISCUSSION

The present paper explores the extent to which cortico-cortical connectivity measures derived from spontaneous ECoG activity resemble cortico-cortical connectivity maps directly documented through cortically-evoked potentials (CEPs). Our results suggest that graph inference measures replicate CEP-resolved connectivity better than coherence measures, a standard neuro-physiological measure for characterizing connectivity.

If two cortical sites are significantly synaptically connected, as evidenced by the presence of a CEP, there will be a higher probability of them being engaged together in a common network during rest or during a task, as evidenced by an overall higher coherence value. The coherence and graph inference measures were computed using spontaneous cortical activity recorded during long periods of time and while the animal was engaged in a variety of behavioral states. In that sense, a higher value in the connectivity maps computed by coherence or graph inference methods could mean that these two cortical sites are more often engaged in synchronous oscillatory networks than two other sites with a lower connectivity value. The level of connectivity changes dynamically with behavioral state, level of attention etc. but an overall trend of higher value of connectivity in the maps computed by coherence or graph inference methods across states may reflect the presence of a stronger functional synaptic projection, captured by a larger CEP which is, overall,

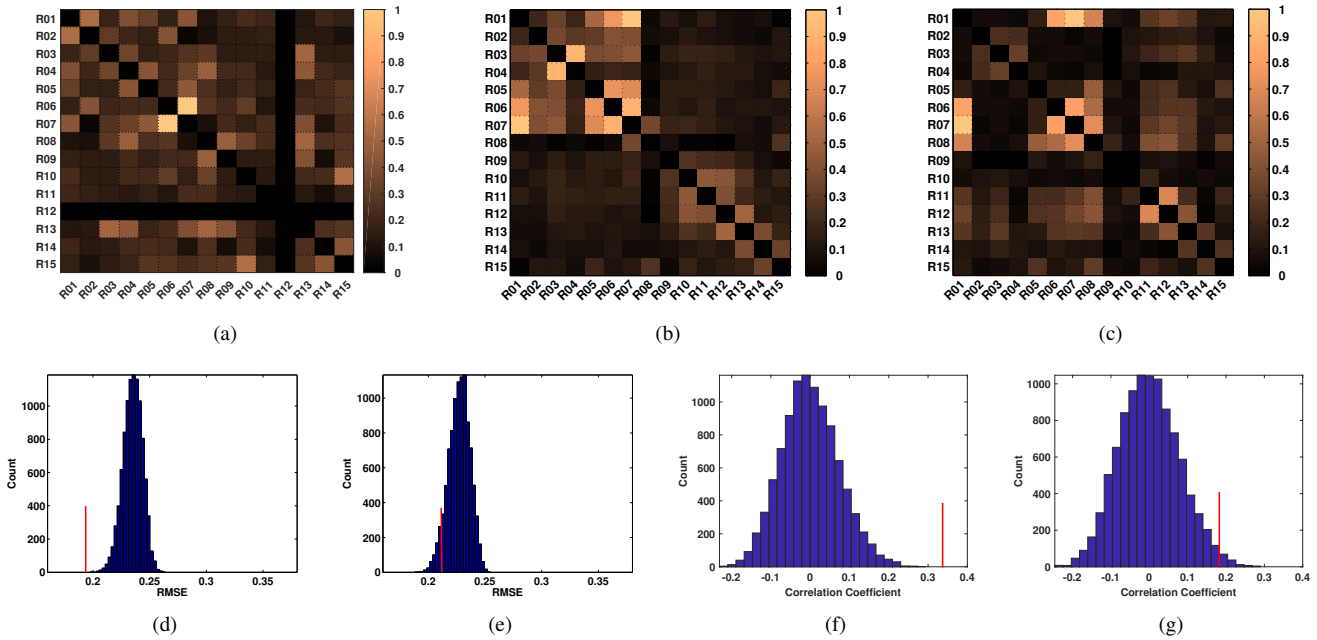

FIGURE 8: Monkey U, Right hemisphere connectivity results: (a) Cortical evoked potential (CEP) connectivity map (b) Cortical connectivity map using graph inference method (c) Cortical connectivity map using spectral coherence method (d) Surrogate maps (error) distribution for RMSE analysis using graph inference method; red line is indicating true RMSE (e) Surrogate maps (error) distribution for RMSE analysis using spectral coherence method; red line is indicating true RMSE (f) Surrogate maps (error) distribution for Correlation analysis using graph inference method; red line is indicating true correlation coefficient (g) Surrogate maps (error) distribution for Correlation Coefficient analysis using spectral coherence method; red line is indicating true correlation coefficient

much more stable across behavioral states.

The graph inference measure uses full spectrum spontaneous recordings of neural data with no *a priori* knowledge of underlying connectivity, which has some advantages. First, it captures relationships across and between all physiologically relevant frequencies and provides a single connectivity value that is frequency-agnostic, compared to methodologies that focus on a single frequency or frequency band, as is the case with coherence. This is important in cases where higher frequency components of neural signals are attenuated or filtered, e.g. due to clinical hardware limitations [19] or in the case of cross-frequency coupling, in which phases of lower frequencies are correlated with the timing and amplitude of higher frequencies [65]. Second, it can be attained without the need for electrical stimulation of the cortex, something that may pose a safety risk in some clinical populations (e.g. epileptic subjects) and is not always experimentally or clinically feasible. Connectivity maps compiled through the CEP method are known to track effects of cortical plasticity paradigms [58]; a reliable method for non-stimulation-based monitoring of connectivity would allow the continuous and long-term quantification of cortical reorganization in health and disease.

Our approach has several limitations. First, connectivity between cortical sites is not always bidirectional or symmetric. In making TRMSE measures across methodologies we made CEP maps symmetric which removes some of the richness of the underlying data (Fig. 2(d)). Second, the analyzed data-set covers only the sensorimotor cortex and not the entire hemisphere. Finally, we have not compared the graph inference measure to infra-slow clustering correlations in high gamma activity, which may be more accurate in capturing underlying anatomical connectivity than coherence [19].

It should be noted that the graph inference method requires a sufficient number of simultaneous recordings from spatially separated sites. It reflects a global relationship that involves activity at sites other than the two sites whose "connectivity" is inferred. This may be the reason why the graph inference method produces a connectivity map more similar to the CEP than coherence measures, since the latter compare signals recorded only at two sites. Single-pulse, biphasic stimulation of the cortical surface activates neurons through several processes [66], [40], [67]. The anodal and cathodal pulses of the electrical stimulus activate different neural elements at the stimulation site. The current depolarizes local pyramidal cell dendrites and axons, local interneurons and other afferent inputs to pyramidal cells, as well as axons of passage. Axons at the stimulation site can be activated both ortho- and antidromically. These processes result in multiple excitatory and inhibitory effects in neurons at the stimulus site. The local responses produce a pattern of action potentials in projection axons that likely have both mono- and poly-synaptic effects on neurons at the recording site,

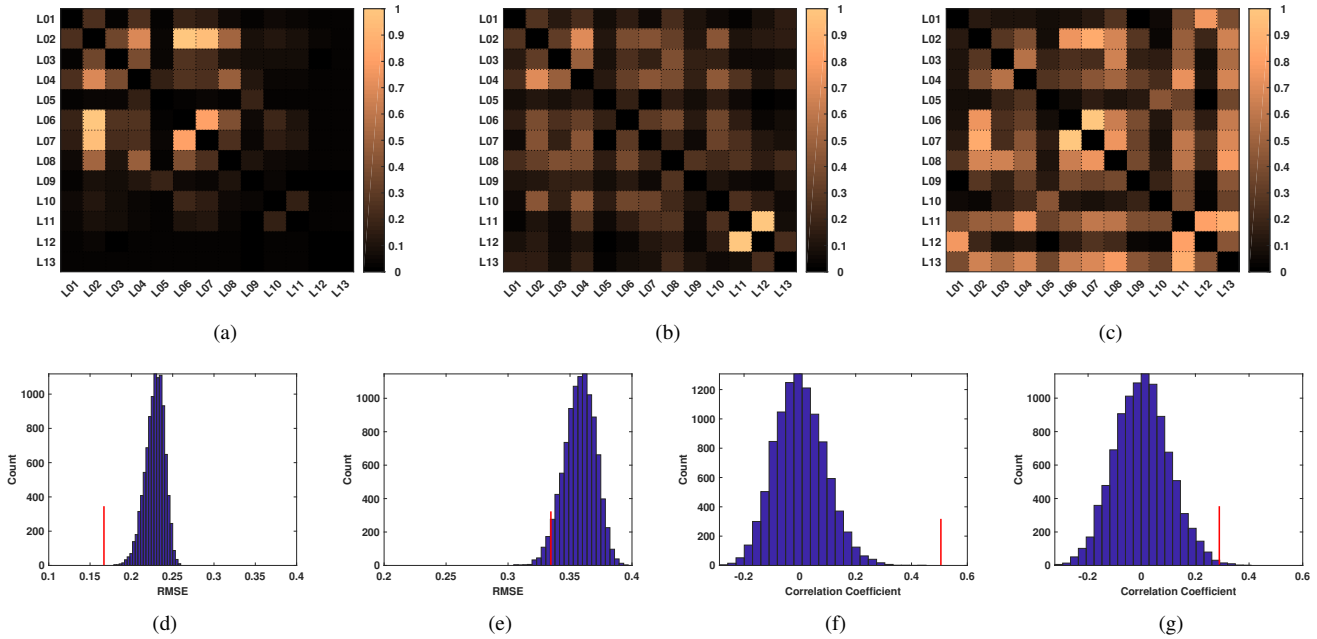

FIGURE 9: Monkey Q, Left hemisphere connectivity results: (a) Cortical evoked potential (CEP) connectivity map (b) Cortical connectivity map using graph inference method (c) Cortical connectivity map using spectral coherence method (d) Surrogate maps (error) distribution for RMSE analysis using graph inference method; red line is indicating true RMSE (e) Surrogate maps (error) distribution for RMSE analysis using spectral coherence method; red line is indicating true RMSE (f) Surrogate maps (error) distribution for Correlation analysis using graph inference method; red line is indicating true correlation coefficient (g) Surrogate maps (error) distribution for Correlation Coefficient analysis using spectral coherence method; red line is indicating true correlation coefficient

which may be mediated by both cortical and subcortical circuits. The compound nature of these interactions generates the multi-phasic population responses that are recorded as CEPs [66], [40], [67]. The earliest responses probably represent monosynaptic projections between the stimulation and recording sites, and longer latency components can be due to conduction in a variety of oligosynaptic pathways. In our own work in non-human primates, we have indirect evidence that cortical evoked potentials are mediated in part by activation of polysynaptic circuits. Paired stimulation protocols can induce spike timing-dependent plasticity in cortico-cortical connections, but only between a subset of tested site pairs [58]. Such specificity is unexpected if CEPs are produced by only monosynaptic connections. We attributed the limited effectiveness of our plasticity protocol to the stimulus-evoked recruitment of multiple cortical circuit effects, which in many cases prevented the expression of a net change in connection strength between cortical sites. In other studies, we demonstrated that CEP amplitude was dependent on the sleep-wake state of the monkey [41], which also suggests the responses are mediated by polysynaptic effects. Because CEPs are mediated by the responses of multiple neurons within at least the local cortical region, measures of connectivity that consider correlated activity across many sites in the region, such as graph inference methods, may provide a good estimate of the functional connectivity revealed by the CEP map. In contrast, single pairwise coherence measures do not account for global correlations of activity and therefore may document a different feature of connectivity.

VII. CONCLUSIONS

The use of graph inference represents a new method that more closely reproduces the synaptic connectivity between cortical sites directly measured from evoked potential recordings than traditional coherence measures. This finding opens the door for a new technique that could closely relay connectivity data in situations where it is impractical to experimentally determine stimulation-based connectivity strengths. This technique can be used to track changes in connectivity over time and understand dynamics of population-scale plasticity and neural dynamics.

REFERENCES

[1] M. D. Fox and M. E. Raichle, "Spontaneous fluctuations in brain activity observed with functional magnetic resonance imaging," Nature Reviews Neuroscience, vol. 8, pp. 700–711, 2007.

[2] K. Friston, "Causal modelling and brain connectivity in functional magnetic resonance imaging," PLoS Biol, vol. 7, no. 2, 2009.

[3] K. E. Stephan and K. J. Friston, "Analyzing effective connectivity with functional magnetic resonance imaging," Wiley Interdisciplinary Reviews: Cognitive Science, vol. 1, no. 3, pp. 446–459, 2010. [Online]. Available: http://dx.doi.org/10.1002/wcs.58

[4] F. D. V. Fallani, L. Astolfi, F. Cincotti, D. Mattia, A. Tocci, S. Salinari, M. G. Marciani, H. Witte, A. Colosimo, and F. Babiloni, "Brain network analysis from high-resolution eeg recordings by the application of theoretical graph indexes," IEEE Transactions on Neural Systems and Rehabilitation Engineering, vol. 16, no. 5, pp. 442–452, Oct 2008.

[5] A. Coito, C. M. Michel, P. van Mierlo, S. Vulliémoz, and G. Plomp, "Directed functional brain connectivity based on eeg source imaging: Methodology and application to temporal lobe epilepsy," IEEE Transactions on Biomedical Engineering, vol. 63, no. 12, pp. 2619–2628, Dec 2016.

[6] N. Hill, D. Gupta, P. Brunner, and et al., "Recording human electrocorticographic (ecog) signals for neuroscientific research and real-time functional cortical mapping." Journal of Visualized Experiments, vol. 64, no. 3993, 2012.

[7] M. A. Kramer, U. T. Eden, E. D. Kolaczyk, R. Zepeda, E. N. Eskandar, and S. S. Cash, "Coalescence and fragmentation of cortical networks during focal seizures," The Journal of Neuroscienc, vol. 30, no. 30, pp. 10 076–10 085, 2010.

[8] F. D. V. Fallani, J. Richiardi, M. Chavez, and S. Achard, "Graph analysis of functional brain networks: practical issues in translational neuroscience," Philosophical Transactions of the Royal Society B: Biological Sciences, 2014.

[9] M. Villafañe-Delgado and S. Aviyente, "Graph information theoretic measures on functional connectivity networks based on graph-to-signal transform," in 2016 IEEE Global Conference on Signal and Information Processing (GlobalSIP), Dec 2016, pp. 1137–1141.

[10] B. He, L. Yang, C. Wilke, and H. Yuan, "Electrophysiological imaging of brain activity and connectivity : Challenges and opportunities," IEEE Transactions on Biomedical Engineering, vol. 58, no. 7, pp. 1918–1931, July 2011.

[11] J. S. Damoiseaux and M. D. Greicius, "Greater than the sum of its parts: a review of studies combining structural connectivity and resting-state functional connectivity," Brain Structure and Function, vol. 213, no. 6, pp. 525–533, Oct 2009. [Online]. Available: https://doi.org/10.1007/s00429-009-0208-6

[12] N.-k. Chen, Y.-h. Chou, A. W. Song, and D. J. Madden, "Measurement of spontaneous signal fluctuations in fmri: adult age differences in intrinsic functional connectivity," Brain Structure and Function, vol. 213, no. 6, pp. 571–585, Oct 2009. [Online]. Available: https://doi.org/10.1007/s00429-009-0218-4

[13] H.-Y. Wey, K. A. Phillips, D. R. McKay, A. R. Laird, P. Kochunov, M. D. Davis, D. C. Glahn, T. Q. Duong, and P. T. Fox, "Multi-region hemispheric specialization differentiates human from nonhuman primate brain function," Brain Structure and Function, vol. 219, no. 6, pp. 2187–2194, Nov 2014. [Online]. Available: https://doi.org/10.1007/s00429-013-0620-9

[14] S. Häkkinen and T. Rinne, "Intrinsic, stimulus-driven and task-dependent connectivity in human auditory cortex," Brain Structure and Function, vol. 223, no. 5, pp. 2113–2127, Jun 2018. [Online]. Available: https://doi.org/10.1007/s00429-018-1612-6

[15] K. R. Patel, S. Tobyne, D. Porter, J. D. Bireley, V. Smith, and E. Klawiter, "Structural disconnection is responsible for increased functional connectivity in multiple sclerosis," Brain Structure and Function, vol. 223, no. 5, pp. 2519–2526, Jun 2018. [Online]. Available: https://doi.org/10.1007/s00429-018-1619-z

[16] P. Stiers and A. Goulas, "Functional connectivity of task context representations in prefrontal nodes of the multiple demand network," Brain Structure and Function, vol. 223, no. 5, pp. 2455–2473, Jun 2018. [Online]. Available: https://doi.org/10.1007/s00429-018-1638-9

[17] G. J. Ortegaa, R. G. Sola, and J. Pastor, "Complex network analysis of human ecog data," Neuroscience Letters, vol. 447, pp. 129 – 133, 2008.

[18] H. Y. Qiao, Z. Zhuo, S. M. Cai, and H. Q. Feng, "Motor-cortical functional connectivity analysis based on ecog signals of finger flexion," in 2010 4th International Conference on Bioinformatics and Biomedical Engineering, June 2010, pp. 1–4.

[19] A. L. Ko, K. E. Weaver, S. Hakimian, and J. G. Ojemann, "Identifying functional networks using endogenous connectivity in gamma band electrocorticography," Brain Connectivity, vol. 3, no. 5, pp. 491–502, 2013.

[20] M. Tanosaki, H. Ishibashi, T. Zhang, and Y. Okada, "Effective connectivity maps in the swine somatosensory cortex estimated from electrocorticography and validated with intracortical local field potential measurements." Brain Connectivity, vol. 4, no. 2, pp. 100 – 111, 2014.

[21] S. Beker, M. Goldin, N. Menkes-Caspi, V. Kellner, G. Chechik, and E. A. Stern, "Amyloid-β disrupts ongoing spontaneous activity in sensory cortex," Brain Structure and Function, vol. 221, no. 2, pp. 1173–1188, Mar 2016. [Online]. Available: https://doi.org/10.1007/s00429-014-0963-x

[22] M. Genetti, R. Tyrand, F. Grouiller, A. Lascano, S. Vulliemoz, L. Spinelli, M. Seeck, K. Schaller, and C. Michel, "Comparison of high gamma electrocorticography and fmri with electrocortical stimulation for localization of somatosensory and language cortex," Clinical Neurophysiology, vol. 126, no. 1, pp. 121–130, 2015.

[23] V. M. Eguíluz, D. R. Chialvo, G. A. Cecchi, M. Baliki, and A. V. Apkarian, "Scale-free brain functional networks," Phys. Rev. Lett., vol. 94, p. 018102, Jan 2005. [Online]. Available: https://link.aps.org/doi/10.1103/PhysRevLett.94.018102

[24] M. Hampson, B. S. Peterson, P. Skudlarski, J. C. Gatenby, and J. C. Gore, "Detection of functional connectivity using temporal correlations in mr images," Human Brain Mapping, vol. 15, no. 4, pp. 247–262, 2002. [Online]. Available: http://dx.doi.org/10.1002/hbm.10022

[25] B. Horwitz, J. M. Rumsey, and B. C. Donohue, "Functional connectivity of the angular gyrus in normal reading and dyslexia," Proceedings of the National Academy of Sciences of the United States of America, vol. 95, no. 15, pp. 8939–8944, 1998.

[26] G. Pfurtscheller and C. Andrew, "Event-related changes of band power and coherence: methodology and interpretation," Journal of Clinical Neurophysiology, vol. 16, 1999.

[27] R. Salvador, J. Suckling, C. Schwarzbauer, and E. Bullmore, "Undirected graphs of frequency-dependent functional connectivity in whole brain networks," Philosophical Transactions of the Royal Society of London B: Biological Sciences, vol. 360, no. 1457, pp. 937–946, 2005. [Online]. Available: http://rstb.royalsocietypublishing.org/content/360/1457/937

[28] Y. Zhang, P. Xu, D. Guo, and D. Yao, "Prediction of ssvep-based bci performance by the resting-state eeg network," Journal of Neural Engineering, vol. 10, 2013.

[29] J. Geweke, "Measurement of linear dependence and feedback between multiple time series," Journal of the American Statistical Association, vol. 77, no. 378, pp. 304–313, 1982. [Online]. Available: http://www.jstor.org/stable/2287238

[30] C. W. J. Granger, "Investigating causal relations by econometric models and cross-spectral methods," Econometrica, vol. 37, no. 3, pp. 424–438, 1969. [Online]. Available: http://www.jstor.org/stable/1912791

[31] M. J. Kaminski and K. J. Blinowska, "A new method of the description of the information flow in the brain structures," Biological Cybernetics, vol. 65, no. 3, pp. 203–210, Jul 1991. [Online]. Available: https://doi.org/10.1007/BF00198091

[32] S. Kelvin, A. C. Koralek, K. Ganguly, M. C. Gastpar, and J. M. Carmena, "Assessing functional connectivity of neural ensembles using directed information," Journal of Neural Engineering, vol. 9, no. 2, 2012.

[33] O. Elzbieta, M. Laura, P. Vittorio, and Z. Filippo, "Comparison of connectivity analyses for resting state eeg data," Journal of Neural Engineering, vol. 14, no. 3, 2017.

[34] A. Roebroeck, E. Formisano, and R. Goebel, "Mapping directed influence over the brain using granger causality and fmri," NeuroImage., vol. 25, no. 1, pp. 230–242, 2005.

[35] D. Rathee, H. Cecotti, and G. Prasad, "Single-trial effective brain connectivity patterns enhance discriminability of mental imagery tasks," Journal of Neural Engineering, vol. 14, no. 5, p. 056005, 2017. [Online]. Available: http://stacks.iop.org/1741-2552/14/i=5/a=056005

[36] A. R. McLntosh and F. Gonzalez-Lima, "Structural equation modeling and its application to network analysis in functional brain imaging," Human Brain Mapping, vol. 2, no. 1-2, pp. 2–22, 1994. [Online]. Available: http://dx.doi.org/10.1002/hbm.460020104

[37] G. Chen, D. R. Glen, Z. S. Saad, J. P. Hamilton, M. E. Thomason, I. H. Gotlib, and R. W. Cox, "Vector autoregression, structural equation modeling, and their synthesis in neuroimaging data analysis," Computers in Biology and Medicine, vol. 41, no. 12, pp. 1142 – 1155, 2011, special Issue on Techniques for Measuring Brain Connectivity. [Online]. Available: http://www.sciencedirect.com/science/article/pii/S0010482511001892

[38] F. Babiloni and J. Gee, "The power of connecting dots: Advanced techniques to evaluate brain functional connectivity in humans," IEEE Transactions on Biomedical Engineering, vol. 63, no. 12, pp. 2447–2449, Dec 2016.

[39] C. J. Keller, C. J. Honey, L. Entz, S. Bickel, D. M. Groppe, E. Toth, I. Ulbert, X. F. A. Lado, and A. D. Mehta, "Corticocortical evoked potentials reveal projectors and integrators in human brain networks," The Journal of Neuroscience,, vol. 34, no. 27, pp. 9152 – 9163, 2014.

[40] C. J. Keller, C. J. Honey, P. MÃl'gevand, L. Entz, I. Ulbert, and A. D. Mehta, "Mapping human brain networks with cortico-cortical evoked potential," Phil. Trans. R. Soc. B, vol. 369, 2014.

[41] A. G. Richardson and E. E. Fetz, "Brain state-dependence of electrically evoked potentials monitoredwith head-mounted electronics," IEEE trans-

actions on neural systems and rehabilitation engineering, vol. 20, no. 6, pp. 756–761, 2012.

[42] A. Sandryhaila and J. M. F. Moura, "Discrete signal processing on graphs," IEEE Transactions on signal processing, vol. 61, no. 7, pp. 1644–1655, 2013.

[43] ——, "Discrete signal processing on graphs: Frequency analysis," IEEE Transactions on signal processing, vol. 62, no. 12, pp. 3042–3054, 2014.

[44] X. Dong, D. Thanou, P. Frossard, and P. Vandergheynst, "Learning laplacian matrix in smooth graph signal representations," IEEE Transactions on Signal Processing, vol. 64, no. 23, pp. 6160–6173, 2016.

[45] S. I. Daitch, J. A. Kelner, and D. A. Spielman, "Fitting a graph to vector data," in Proceedings of the 26th Annual International Conference on Machine Learning, ser. ICML '09. New York, NY, USA: ACM, 2009, pp. 201–208. [Online]. Available: http://doi.acm.org/10.1145/1553374.1553400

[46] S. Chepuri, S. Liu, G. Leus, and A. Hero, "Learning sparse graphs under smoothness prior," in 2017 IEEE International Conference on Acoustics, Speech, and Signal Processing, ICASSP 2017 - Proceedings. Institute of Electrical and Electronics Engineers Inc., 6 2017, pp. 6508–6512.

[47] H. E. Egilmez, E. Pavez, and A. Ortega, "Graph learning from data under laplacian and structural constraints," IEEE Journal of Selected Topics in Signal Processing, vol. 11, no. 6, pp. 825–841, Sept 2017.

[48] S. Segarra, A. G. Marques, G. Mateos, and A. Ribeiro, "Network topology inference from spectral templates," IEEE Transactions on Signal and Information Processing over Networks, vol. 3, no. 3, pp. 467–483, Sept 2017.

[49] B. Pasdeloup, V. Gripon, G. Mercier, D. Pastor, and M. G. Rabbat, "Characterization and inference of graph diffusion processes from observations of stationary signals," IEEE Transactions on Signal and Information Processing over Networks, 2017.

[50] R. Shafipour, S. Segarra, A. G. Marques, and G. Mateos, "Identifying the topology of undirected networks from diffused non-stationary graph signals," CoRR, vol. abs/1801.03862, 2018.

[51] S. Colonnese, G. Pagliari, M. Biagi, and R. Cusani, "Compound markov random field model of signals on graph: An application to graph learning," in 2018 7th European Workshop on Visual Information Processing (EUVIP), 11 2018, pp. 1–5.

[52] G. Mateos, S. Segarra, A. G. Marques, and A. Ribeiro, "Connecting the dots: Identifying network structure via graph signal processing," IEEE Signal Processing Magazine, vol. 36, no. 3, pp. 16–43, May 2019.

[53] X. Dong, D. Thanou, M. Rabbat, and P. Frossard, "Learning graphs from data: A signal representation perspective," IEEE Signal Process. Mag., vol. 36, no. 3, pp. 44–63, 2019. [Online]. Available: https://doi.org/10.1109/MSP.2018.2887284

[54] K. Stephan, C. Hilgetag, G. Burns, M. O'Neill, M. Young, and R. KÃűtter, "Computational analysis of functional connectivity between areas of primate cerebral cortex," Philosophical transactions of the Royal Society of London. Series B, Biological sciences, vol. 355, no. 1393, p. 111âĂŤ126, January 2000. [Online]. Available: http://europepmc.org/articles/PMC1692715

[55] C. Stam, "Functional connectivity patterns of human magnetoencephalographic recordings: a âĂŸsmall-worldâĂŹ network?" Neuroscience Letters, vol. 355, no. 1, pp. 25 – 28, 2004. [Online]. Available: http://www.sciencedirect.com/science/article/pii/S0304394003012722

[56] R. Salvador, J. Suckling, M. R. Coleman, J. D. Pickard, D. Menon, and E. Bullmore, "Neurophysiological Architecture of Functional Magnetic Resonance Images of Human Brain," Cerebral Cortex, vol. 15, no. 9, pp. 1332–1342, 01 2005. [Online]. Available: https://doi.org/10.1093/cercor/bhi016

[57] M. A. Guevara and M. Corsi-Cabrera, "Eeg coherence or eeg correlation?" International Journal of Psychophysiology, vol. 23, no. 3, pp. 145 – 153, 1996. [Online]. Available: http://www.sciencedirect.com/science/article/pii/S0167876096000384

[58] S. C. Seeman, B. J. Mogen, E. E. Fetz, and S. I. Perlmutter, "Paired stimulation for spike-timing dependent plasticity in primate sensorimotor cortex," Journal of Neuroscience, 2017. [Online]. Available: http://www.jneurosci.org/content/early/2017/01/16/JNEUROSCI.2046-16.2017

[59] G. Buzsáki and A. Draguhn, "Neuronal oscillations in cortical networks," Science, vol. 304, no. 5679, pp. 1926–1929, 2004. [Online]. Available: http://science.sciencemag.org/content/304/5679/1926

[60] F. Mormann, K. Lehnertz, P. David, and C. E. Elger, "Mean phase coherence as a measure for phase synchronization and its application to the eeg of epilepsy patients," Physica D: Nonlinear Phenomena, vol. 144, no. 3, pp. 358 – 369, 2000. [Online]. Available: http://www.sciencedirect.com/science/article/pii/S0167278900000877

[61] C. J. Stam, G. Nolte, and A. Daffertshofer, "Phase lag index: Assessment of functional connectivity from multi channel eeg and meg with diminished bias from common sources," Human Brain Mapping, vol. 28, no. 11, pp. 1178–1193, 2007. [Online]. Available: http://dx.doi.org/10.1002/hbm.20346

[62] H. Akaike, "A new look at the statistical model identification," IEEE Transactions on Automatic Control, vol. 19, no. 6, pp. 716–723, Dec 1974.

[63] C. Herrmann, M. Barthélemy, and P. Provero, "Connectivity distribution of spatial networks," Phys. Rev. E, vol. 68, p. 026128, Aug 2003. [Online]. Available: https://link.aps.org/doi/10.1103/PhysRevE.68.026128

[64] B. Efron, "Nonparametric estimates of standard error: The jackknife, the bootstrap and other methods," Biometrica, vol. 68, pp. 589–599, 1981.

[65] R. T. Canolty and R. T. Knight., "The functional role of cross-frequency coupling," Trends in Cognitive Sciences, vol. 14, no. 11, pp. 506–515, 2010.

[66] R. Matsumoto, D. R. Nair, E. LaPresto, W. Bingaman, H. Shibasaki, and H. O. LÃijders, "Functional connectivity in human cortical motor system: a cortico-cortical evoked potential study," Brain, vol. 130, no. 1, pp. 181–197, 2007. [Online]. Available: http://dx.doi.org/10.1093/brain/awl257

[67] T. KUNIEDA, Y. YAMAO, T. KIKUCHI, and R. MATSUMOTO, "New approach for exploring cerebral functional connectivity: Review of cortico-cortical evoked potential," Neurologia medico-chirurgica, vol. 55, no. 5, pp. 374–382, 2015.

SIDDHI TAVILDAR received the B.E. degree in Electronics Engineering from Pune University, Maharashtra, India, in 2010 and the M.S. degree in Electrical Engineering from San Diego State University, San Diego, CA, in 2014. She is currently pursuing the Ph.D. degree in Computational Sciences at San Diego State University, San Diego, CA, USA.

She is currently working as a Research Assistant at the Signal Processing Research Laboratory in San Diego State University, San Diego, CA. Her research interest includes bio-medical signal processing, graph theory and graph signal processing.

BRIAN MOGEN received the B.S. degree in Biomedical Engineering from University of Wisconsin-Madison, WI in 2011, and the Ph.D. degree in Bioengineering from the University of Washington, Seattle, WA in 2018.

STEPHANIE C. SEEMAN received the B.S. degree in Biology and Chemistry from Union College, Schenectady, NY in 2008, and the Ph.D. degree in Neuroscience from the University of Washington, Seattle, WA in 2016.

Currently she is working at the Allen Institute for Brain Science in Seattle, WA. Her current research is focused on understanding the unique connectivity of cell types and how this drives behavior.

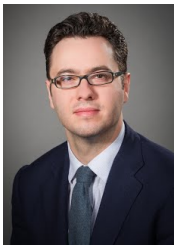

STAVROS ZANOS obtained his MD diploma from Aristotle University, in Thessaloniki, Greece. He served as a general medical practitioner and a military physician, before training in internal medicine at the Papageorgiou General Hospital, in Thessaloniki, Greece and in cardiology at the Onassis Cardiac Surgery Center, in Athens, Greece. He earned his PhD in Neuroscience and Physiology from the University of Washington School of Medicine in 2013, where he also served as senior fellow and instructor.

He joined the Feinstein Institute for Medical Research as assistant professor in 2017.

STEVE I. PERLMUTTER received an Sc.B from Brown University in Biomedical Engineering in 1979, an M.S. from UCLA in Biomedical Engineering in 1982, and a Ph.D. in Physiology and Neuroscience from Northwestern University in 1991.

He is currently a Research Associate Professor in the Department of Physiology & Biophysics at the University of Washington, a Research Affiliate at the Washington National Primate Research Center, and a member of the Center for Neurotechnology and the University of Washington Institute for Neuroengineering. His research interests include spinal control of voluntary movements, neural plasticity, and neuroprosthetics. His lab is developing therapies for spinal cord injury and stroke that use activity-dependent, targeted, electrical and optical stimulation of the nervous system.

EBERHARD FETZ received his B.S. in physics from the Rensselaer Polytechnic Institute in 1961, and his Ph.D. in physics from the Massachusetts Institute of Technology in 1967. He came to the University of Washington for postdoctoral work in neuroscience and has been on the faculty ever since.

He is currently Professor in the Department of Physiology & Biophysics and core staff of the Washington National Primate Research Center. He is also a member of Center for Neurotechnology.

ASHKAN ASHRAFI (M'98-S'02-M'06-SM'08) received his BSc and MSc degrees in Electronics Engineering from K.N. Toosi University of Technology, Tehran, Iran and MSE and Ph.D. degrees in Electrical Engineering from the University of Alabama in Huntsville, Huntsville, AL, USA in 1991, 1995, 2003 and 2006, respectively (all with the highest honor). He is currently an Associate Professor of Electrical and Computer Engineering at San Diego State University, San Diego, CA where he is also the director of the Signal Processing Research Laboratory. His research interests are digital and statistical signal processing, graph theory and graph signal processing, estimation theory, bio-medical signal processing, brain connectivity analysis and audio processing.

He is the recipient of the Outstanding Faculty Award of the Department of Electrical and Computer Engineering, San Diego State University in both 2012 and 2013. He served as an associate editor for IEEE Transactions on Circuits and Systems Part-I: Regular Papers between 2011 and 2014 and received the Best Associate Editor Award in 2013. He is a member of Phi-Kappa-Phi, Sigma-Xi and Eta-Kappa-Nu honor societies.